JACS
JOURNAL OF THE AMERICAN CHEMICAL SOCIETY
Communication
pubs.acs.org/JACS

Efficient Electrocatalytic Oxidation of Formic Acid Using Au@Pt Dendrimer-Encapsulated Nanoparticles

Ravikumar Iyyamperumal,[†,‡] Liang Zhang,[†,‡,§] Graeme Henkelman,*[,†,‡,§] and Richard M. Crooks*[,†,‡]

[†]Department of Chemistry and Biochemistry, [‡]Texas Materials Institute, and [§]Institute for Computational and Engineering Sciences, The University of Texas at Austin, 105 East 24th Street, Stop A5300, Austin, Texas 78712-1224, United States

Supporting Information

ABSTRACT: We report electrocatalytic oxidation of formic acid using monometallic and bimetallic dendrimer-encapsulated nanoparticles (DENs). The results indicate that the Au_{147}@Pt DENs exhibit better electrocatalytic activity and low CO formation. Theoretical calculations attribute the observed activity to the deformation of nanoparticle structure, slow dehydration of formic acid, and weak binding of CO on Au_{147}@Pt surface. Subsequent experiments confirmed the theoretical predictions.

In this Communication we show that electrochemically synthesized nanoparticles consisting of a 147-atom Au core and a Pt shell (Au_{147}@Pt) facilitate the direct oxidation of formic acid to carbon dioxide. Specifically, experiments and first-principles calculations show that ~2-nm-diameter Au_{147}@Pt dendrimer-encapsulated nanoparticles (DENs)[1] undergo a structural distortion that suppresses formation of adsorbed CO (CO_{ads}) compared to Pt-only DENs.[2] This finding is significant, because it represents an unusual case in which a well-defined structural deformation of a very small nanoparticle results in a dramatic improvement in catalytic performance.

Formic acid is used as a substitute fuel for hydrogen in proton exchange membrane fuel cells (PEMFCs), because oxidation of hydrogen and formic acid occurs at similar thermodynamic potentials.[3] Electro-oxidation of HCOOH to CO_2 on Pt electrocatalysts occurs via two mechanisms: (1) through formation of a reactive intermediate (direct oxidation pathway), and (2) through formation of CO_{ads} and subsequent oxidation of CO_{ads} to CO_2 (indirect oxidation pathway).[4] The second pathway is problematic, because CO_{ads} poisons the Pt surface. However, it has been shown that the presence of Au can improve the CO tolerance of Pt, and hence its catalytic performance.[5−7] For example, Xu and co-workers found that Au@Pt nanoparticles having submonolayer Pt shells exhibit improved electrocatalytic activity for formic acid oxidation due to specifically engineered electronic interactions between the two metals.[8] An alternative to improving CO tolerance is to simply avoid CO altogether. For example, Masel and co-workers found that carbon-supported Pd is highly active for formic acid oxidation, because it favors the direct oxidation pathway.[9] However, Pd/C suffers significant loss in activity during formic acid oxidation due to slow adsorption of CO-like intermediates, bridge-bonded formate, perchlorate, and other anions.[10]

The DENs in this study were synthesized, and their structure characterized, using methods we previously reported.[11−13] Briefly, Pt_{147} DENs were synthesized by adding 147 equiv of K_2PtCl_4 to a 2.0 μM aqueous solution of a sixth-generation, hydroxyl-terminated poly(amidoamine) dendrimer (G6-OH). The Pt^{2+} was allowed to complex with the dendrimer for 3 days, and then a 10-fold excess of $NaBH_4$ was added to reduce the G6-OH$(Pt^{2+})_{147}$ precursor to G6-OH(Pt_{147}) DENs. A similar procedure was used for the synthesis of Au_{147} DENs, except the reduction was initiated almost immediately after addition of $HAuCl_4$ to avoid competitive reduction by the hydroxyl groups of the dendrimers. Pt and Au DEN-modified electrodes were prepared by sonicating an aqueous solution, containing 20% isopropyl alcohol, with 2 mg mL^{-1} of Vulcan EC-72R carbon for 5 min, and then drop-casting 4.0 μL of the resulting ink onto a freshly polished glassy carbon electrode (GCE). The electrode was then dried at room temperature. Following a method pioneered by Adzic and co-workers,[14] and our previous experimental procedure,[12] Au_{147}@Pt DENs were synthesized by electrochemical underpotential deposition (UPD) of Pb onto Au_{147} DENs, followed by galvanic exchange with $PtCl_4^{2-}$. Specifically, Au_{147} DENs were immobilized on a GCE, and then a monolayer of Pb was added to the Au core by UPD from a N_2-saturated aqueous solution containing 1.0 mM $Pb(NO_3)_2$ and 0.10 M $HClO_4$. Next, 10.0 mL of a 1.0 mM K_2PtCl_4 solution was added to initiate galvanic exchange of Pb for Pt. The resulting DENs were then characterized by UV−vis spectroscopy, transmission electron microscopy, and electrochemical methods (Supporting Information) and found to be consistent with our previous findings.[12]

Figure 1 shows cyclic voltammograms (CVs) for formic acid oxidation using Au_{147}, Pt_{147}, and Au_{147}@Pt DEN-modified GCEs in 0.10 M $HClO_4$ containing 0.10 M HCOOH. The Au_{147} DENs do not exhibit detectable activity for formic acid oxidation. In contrast, the Pt_{147} DEN-modified electrode reveals two peaks at −0.12 and 0.21 V (vs Hg/Hg_2SO_4) in the scan toward more positive potentials. These are attributable to the direct oxidation of HCOOH to CO_2 and oxidation of CO_{ads}, generated by dehydration of HCOOH, respectively.[15] The low ratio (2.8) of the current densities (j_p^d/j_p^{ind}, Table 1) for these two peaks indicates a substantial degree of indirect electrocatalytic oxidation of formic acid on Pt_{147} DENs.[16] Upon scan reversal, a single peak is observed at −0.24 V, which corresponds to direct oxidation of HCOOH to CO_2. With

Received: January 29, 2013
Published: April 8, 2013

dx.doi.org/10.1021/ja4010305 | J. Am. Chem. Soc. 2013, 135, 5521−5524

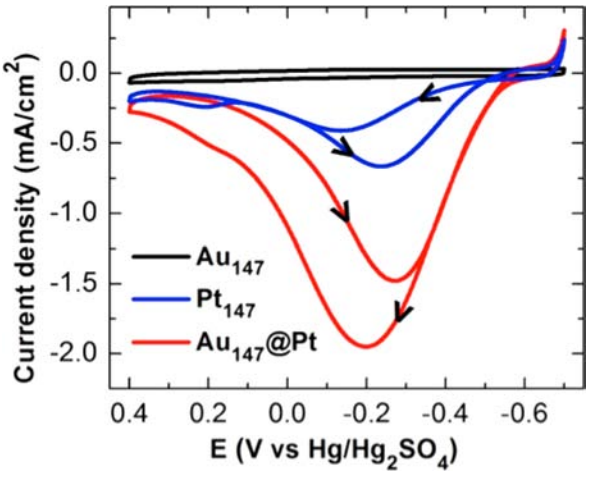

Figure 1. CVs for formic acid oxidation of Au_{147}, Pt_{147}, and Au_{147}@Pt DEN-modified GCEs in a N_2-saturated aqueous electrolyte solution containing 0.10 M $HClO_4$ and 0.10 M HCOOH. The scan rate was 50 mV/s, and the geometric area of the GCE was 0.071 cm^2. For the Pt_{147} and Au_{147}@Pt DENs, the current axis is normalized to the electrochemically active surface area of Pt as measured by H UPD. For the Au_{147} DENs, the current is normalized to the electrochemically active surface area of Au as measured by reduction of the Au oxide peak.

the exception of the peak potential on the reverse scan, which is shifted positive by about 60 mV, these peak potentials are in nearly the same positions as those obtained using a macroscopic polycrystalline Pt electrode under the same experimental conditions (Supporting Information).[15]

The Au_{147}@Pt DEN electrocatalysts display superior catalytic performance compared to the Pt_{147} DENs and a bulk, polycrystalline Pt electrode. This is demonstrated by the red CV shown in Figure 1. There are four striking differences between this CV and the Pt-only CVs (Pt_{147} DENs and the bulk, polycrystalline Pt electrode, Figure S5). First, the peak at ~0.2 V, which corresponds to oxidation of CO_{ads}, is nearly absent on the Au_{147}@Pt DENs. The fact that very little CO_{ads} on the bimetallic DENs indicates that formic acid is oxidized almost exclusively via the direct pathway on this electrocatalyst. Second, the Au_{147}@Pt electrocatalyst exhibits an onset potential (defined here as the potential at which the current density = 0.10 mA/cm^2)[17] for formic acid oxidation of −0.54 V, which is 0.14 and 0.20 V lower than for Pt_{147} DENs and a polycrystalline Pt electrode, respectively. Third, the maximum current density (j_p^d) for direct formic acid oxidation is substantially higher for the Au_{147}@Pt DENs compared to either Pt_{147} DENs or the bulk, polycrystalline Pt electrode (note that the currents in Table 1 and Figure 1 are normalized to the electrochemically active surface areas of Pt). This level of catalytic performance is also substantially better than that observed using Pd black on carbon (Table 1).[18] The increased activity of the Au_{147}@Pt DENs results from the desirable electronic properties of the core@shell structure. Fourth, the peak current for the forward (positive-going) scan for the Au_{147}@Pt DENs is higher than for the reverse scan, which is the opposite of what is observed for the Pt_{147} DENs and for a bulk polycrystalline electrode (Figure S5). This is a consequence of a decrease in CO poisoning at the more negative potentials and differences in the rate of oxide formation and subsequent reduction at more positive potentials.

As mentioned previously, one of the most distinctive features of formic acid oxidation on Au_{147}@Pt DENs is near-elimination of the indirect formic acid oxidation pathway. We hypothesized that the reduction in CO poisoning could arise from either of the following phenomena: (1) slowed dehydration of HCOOH, which eliminates formation of CO, or (2) weakening of the CO binding energy. With regard to the first hypothesis, Yancey et al. proposed a deformed partial shell (dps) model for Au_{147}@Pt DENs.[12] These materials, which we denote as Au@Pt_{dps}, are the same as those used in the present study (Figure 2).[12] In this model, a surface distortion was observed during molecular dynamics simulations in which the Pt-covered (100) facets sheared into a diamond (111) structure. This distortion may play an important role in the rate of dehydration of HCOOH to CO on the DENs, because formation of CO during formic acid oxidation on Pt(111) single-crystal electrodes is not favorable.[19,20]

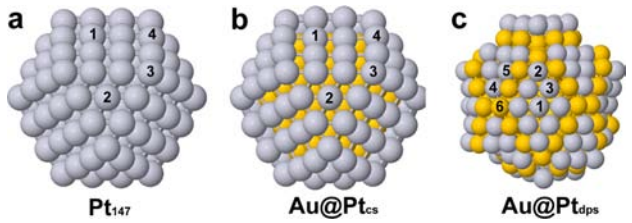

Figure 2. Optimized structures for (a) the Pt-only DEN model (Pt_{147}), (b) the complete shell model (Au@Pt_{cs}), which is equivalent to Au_{55}@Pt_{92}, and (c) the deformed partial-shell model (Au@Pt_{dps}), which is equivalent to Au_{147}@Pt_{102}. The superimposed numbers represent possible CO binding sites for each model.

The second hypothesis was tested using DFT to calculate the CO binding energies on Pt_{147}, the Au@Pt_{dps} model, and a complete shell model of Au@Pt (Au@Pt_{cs}). These three structures, showing possible CO binding sites, are provided in

Table 1. Electrochemical Parameters for Formic Acid Oxidation Derived from Figure 1

	onset potential (V)[a]	peak potential[b] (V)		current density[c] (mA/cm^2)		ratio j_p^d/j_p^{ind}
		E_p^d	E_p^{ind}	j_p^d	j_p^{ind}	
Pt (polycrystalline)	−0.34	−0.13	0.15	0.90	0.52	1.7
G6-OH(Pt_{147})	−0.40	−0.12	0.21	0.36	0.13	2.8
G6-OH(Au_{147}@Pt)	−0.54	−0.20	0.20	1.91	0.07	27.3
Pd black[18]	−0.44	0.06		1.35		

[a]The onset potentials are defined as the potential corresponding to formic acid oxidation at a current density of 0.10 mA/cm^2.[17] [b]E_p^d and E_p^{ind} are the potentials corresponding to the maximum currents for the positive-going scans in Figure 1. [c]j_p^d and j_p^{ind} are the peak current densities corresponding to E_p^d and E_p^{ind}, respectively. These values are normalized to the true area of Pt determined by hydrogen UPD. The current density is also normalized for the true surface area of Pd.

dx.doi.org/10.1021/ja4010305 | J. Am. Chem. Soc. 2013, 135, 5521−5524

Table 2. CO Binding Energies for Different Sites on the Pt_{147}, $Au_{55}@Pt_{92}$, and $Au_{147}@Pt_{102}$ Model

Pt-only model (Pt_{147})			complete shell ($Au@Pt_{cs}$) model ($Au_{55}@Pt_{92}$)			deformed partial shell ($Au@Pt_{dps}$) model ($Au_{147}@Pt_{102}$)		
	binding site	BE_CO (eV)		binding site	BE_CO (eV)		binding site[a]	BE_CO (eV)
1	(100)	−3.12	1	(100)	−3.34	1	D(111) center	−1.74
2	(111)	−2.65	2	(111)	−3.07	2	D(111) corner	−1.96
3	corner	−3.30	3	corner	−3.36	3	D(111) edge	−1.80
4	edge	−3.15	4	edge	−3.40	4	T(111) corner	−1.44
						5	T(111) edge	−1.37
						6	Au	−0.47

[a]D(111) and T(111) denote the diamond (111) and triangle (111) facets, respectively.

Figure 2, and the corresponding CO binding energies are listed in Table 2. The results indicate that $Au@Pt_{cs}$ binds CO more strongly than Pt_{147}, which is in agreement with results from previous DFT calculations on bulk model surfaces and with temperature-programmed desorption experiments.[21] Importantly, however, the binding energy calculations reveal significant weakening of CO binding to $Au@Pt_{dps}$. These CO binding trends can be interpreted in terms of the average Pt−Pt bond lengths in the different models: $Au@Pt_{cs}$, 2.79 Å; Pt_{147}, 2.76 Å; and $Au@Pt_{dps}$, 2.65 Å. The compression of the Pt−Pt bond in $Au@Pt_{dps}$ leads to weaker binding of CO on the Pt surface compared to either Pt_{147} or $Au@Pt_{cs}$ DENs.[21]

On the basis of the foregoing discussion, we conclude that weakened CO binding and slow dehydration of HCOOH on the $Au_{147}@Pt$ surface account for reduced CO poisoning and the enhanced activity of this catalyst for formic acid oxidation. To test these conclusions experimentally, two different CO oxidation experiments were performed using GCEs modified with Pt_{147} and $Au_{147}@Pt$ DENs (Figure 3). For the first experiment, the DEN-modified electrodes were each immersed in a solution containing 0.10 M $HClO_4$ and 0.10 M HCOOH for 5 min at open-circuit potential (OCP). This results in chemisorption of CO arising from dehydration of HCOOH.[19,22] The electrode was then removed from the formic acid solution, washed, and placed in a fresh solution containing only N_2-purged 0.10 M $HClO_4$, and then CVs were obtained. In the case of Pt_{147} DENs (Figure 3a), a broad peak is observed at ∼0.10 V during the first scan toward positive potentials. We attribute this peak to oxidation of CO_{ads}. However, no corresponding peak for oxidation of CO_{ads} is observed for the $Au_{147}@Pt$ DENs. These results indicate that dehydration of HCOOH to CO_{ads} is slower on $Au_{147}@Pt$ DENs than Pt_{147} DENs surfaces, which is consistent with the calculations alluded to earlier.

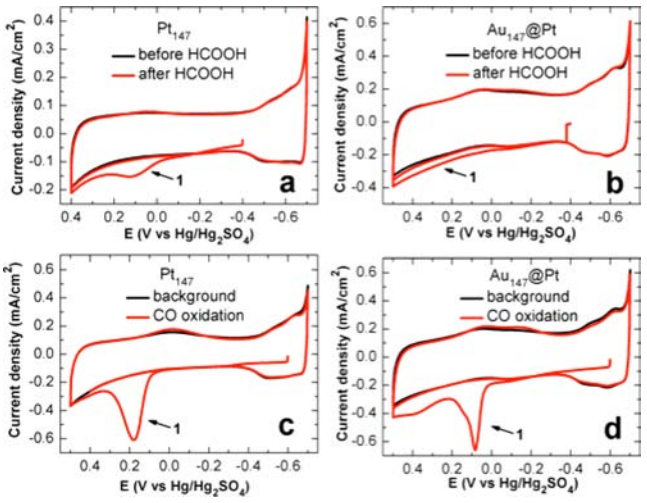

Figure 3. The red CVs show oxidation of CO_{ads} on Pt_{147}- and $Au_{147}@$Pt-modified GCEs (peaks indicated by "1"). (a,b) The DEN-modified electrodes were exposed to an aqueous solution containing 0.10 M $HClO_4$ and 0.10 M HCOOH for 5 min at the open circuit potential (OCP), rinsed in water, and then placed in a HCOOH-free, 0.10 M $HClO_4$ solution for electrochemical analysis. (c,d) The DEN-modified electrodes were immersed in a CO-saturated, aqueous 0.10 M $HClO_4$ electrolyte solution and held at a potential of −0.60 V for 10 min. Without changing the electrode potential, the solution was then purged with N_2, and the CVs were recorded. The black curves are control experiments in which the electrodes were not exposed to CO or HCOOH. The scan rate was 50 mV/s, and the geometric area of the GCE was 0.071 cm^2.

The second experiment was carried out by immersing the DEN-modified GCEs in a CO-saturated aqueous 0.10 M $HClO_4$ electrolyte solution for 10 min at −0.60 V (rather than at the OCP). These conditions result in formation of a strongly adsorbed monolayer of CO on the surface of the DENs. The electrolyte solution was then purged with N_2 for 10 min, while maintaining the electrode potential at −0.60 V, to remove dissolved CO. Finally, CVs were obtained. For the Pt_{147}-modified electrode, a large oxidation wave attributable to CO oxidation is observed at ∼0.20 V (Figure 3c). A similar peak, but shifted negative by about 100 mV, is observed for the $Au_{147}@Pt$ DENs (Figure 3d). This shift indicates that CO adsorbs more weakly to the bimetallic DENs, which, again, is consistent with the binding energies obtained from DFT calculations. Taken together, the experiments summarized in Figure 3 and the DFT calculations strongly suggest that the high catalytic activity and small extent of CO poisoning, revealed by the CVs in Figure 1, arise from both slow dehydration of formic acid and weak binding of CO on the $Au_{147}@Pt$ DENs.

In conclusion, we have shown that $Au_{147}@Pt$ DENs exhibit better electrocatalytic activity for HCOOH oxidation reaction than Pt_{147} DENs, a bulk, polycrystalline Pt electrode, and carbon-supported Pd black. DFT calculations provide an explanation for these findings that is fully consistent with the experiments. Specifically, the $Au_{147}@Pt$ DENs undergo a structural transition (Figure 2) that leads to both slower dehydration of formic acid and weaker binding of CO_{ads}. Perhaps the most significant outcome of this work, however, is that there appear to be major structural differences between particles in the 1−2 nm size range of DENs, and the more commonly studied (and more experimentally tractable) nanoparticles having sizes >3 nm. This is likely due to the lower stability of the smaller particles, and thus their enhanced ability to deform in the presence of adsorbates and during catalysis. In forthcoming publications we will show that this is a rather

dx.doi.org/10.1021/ja4010305 | J. Am. Chem. Soc. 2013, 135, 5521−5524

general result that deserves more attention than it has thus far received.

■ ASSOCIATED CONTENT

Supporting Information

Detailed experimental procedures, TEM images and particle-size distributions, details of the DFT calculations, CVs for Pt_{147} and Au_{147}@Pt DENs before and after formic acid oxidation, and CV of a bulk, polycrystalline Pt electrode in the presence and absence of formic acid. This material is available free of charge via the Internet at http://pubs.acs.org.

■ AUTHOR INFORMATION

Corresponding Author

crooks@cm.utexas.edu; henkelman@cm.utexas.edu

Notes

The authors declare no competing financial interest.

■ ACKNOWLEDGMENTS

We gratefully acknowledge support from the Chemical Sciences, Geosciences, and Biosciences Division, Office of Basic Energy Sciences, Office of Science, U.S. Department of Energy (Contract DE-FG02-09ER16090). R.M.C. also thanks the Robert A. Welch Foundation (Grant F-0032) for sustained support. The computational work was done primarily at the National Energy Research Scientific Computing Center and the Texas Advanced Computing Center. Finally, we thank Mr. David Yancey (UT-Austin) and Prof. Carol Korzeniewski (Texas Tech University) for helpful discussions.

■ REFERENCES

(1) Myers, V. S.; Weir, M. G.; Carino, E. V.; Yancey, D. F.; Pande, S.; Crooks, R. M. *Chem. Sci.* **2011**, *2*, 1632−1646.

(2) Ye, H.; Crooks, J. A.; Crooks, R. M. *Langmuir* **2007**, *23*, 11901−11906.

(3) Weber, M.; Wang, J.-T.; Wasmus, S.; Savinell, R. F. *J. Electrochem. Soc.* **1996**, *143*, L158−L160.

(4) Capon, A.; Parson, R. *J. Electroanal. Chem. Interfacial Electrochem.* **1973**, *44*, 1−7.

(5) Kristian, N.; Yan, Y.; Wang, X. *Chem. Commun.* **2008**, 353−355.

(6) Park, I.-S.; Lee, K.-S.; Choi, J.-H.; Park, H.-Y.; Sung, Y.-E. *J. Phys. Chem. C* **2007**, *111*, 19126−19133.

(7) Zhang, S.; Shao, Y.; Liao, H.-g.; Liu, J.; Aksay, I. A.; Yin, G.; Lin, Y. *Chem. Mater.* **2011**, *23*, 1079−1081.

(8) Zhang, G.-R.; Zhao, D.; Feng, Y.-Y.; Zhang, B.; Su, D. S.; Liu, G.; Xu, B.-Q. *ACS Nano* **2012**, *6*, 2226−2236.

(9) Rice, C.; Ha, S.; Masel, R. I.; Waszczuk, P.; Wieckowski, A.; Barnard, T. *J. Power Sources* **2002**, *111*, 83−89.

(10) Yu, X.; Pickup, P. G. *Electrochem. Commun.* **2009**, *11*, 2012−2014.

(11) Kim, Y.-G.; Oh, S.-K.; Crooks, R. M. *Chem. Mater.* **2003**, *16*, 167−172.

(12) Yancey, D. F.; Zhang, L.; Crooks, R. M.; Henkelman, G. *Chem. Sci.* **2012**, *3*, 1033−1040.

(13) Ye, H.; Crooks, R. M. *J. Am. Chem. Soc.* **2005**, *127*, 4930−4934.

(14) Sasaki, K.; Wang, J. X.; Naohara, H.; Marinkovic, N.; More, K.; Inada, H.; Adzic, R. R. *Electrochim. Acta* **2010**, *55*, 2645−2652.

(15) Parsons, R.; VanderNoot, T. *J. Electroanal. Chem. Interfacial Electrochem.* **1988**, *257*, 9−45.

(16) Chen, W.; Xu, L.-P.; Chen, S. *J. Electroanal. Chem.* **2009**, *631*, 36−42.

(17) Kanan, M. W.; Nocera, D. G. *Science* **2008**, *321*, 1072−1075.

(18) Haan, J. L.; Masel, R. I. *Electrochim. Acta* **2009**, *54*, 4073−4078.

(19) Maciá, M. D.; Herrero, E.; Feliu, J. M. *Electrochim. Acta* **2002**, *47*, 3653−3661.

(20) Rhee, C. K.; Kim, B.-J.; Ham, C.; Kim, Y.-J.; Song, K.; Kwon, K. *Langmuir* **2009**, *25*, 7140−7147.

(21) Friedrich, K. A.; Henglein, F.; Stimming, U.; Unkauf, W. *Electrochim. Acta* **2000**, *45*, 3283−3293.

(22) Sun, S. G.; Clavilier, J. *J. Electroanal. Chem. Interfacial Electrochem.* **1987**, *236*, 95−112.